Performance Analysis of Alamouti-Coded OFDM Systems Over Spatio-Temporally Correlated Underwater Acoustic Channels

Meisam Naderi[1], Gulzaib Rafiq[2], and Matthias Pätzold[1]

[1]*Faculty of Engineering and Science, University of Agder, P.O. Box 509, 4879 Grimstad, Norway*
[2]*ABB Corporate Research Center, Billingstad NO-1396, Norway*
Emails: [1]{meisam.naderi, matthias.paetzold}@uia.no, [2]gulzaib.rafiq@no.abb.com

Abstract—In this paper, we analyze the performance of Alamouti-coded orthogonal frequency division multiplexing (OFDM) systems over time-varying underwater acoustic (UWA) channels. A realistic UWA channel model has been considered, which can be correlated in either time or space or simultaneously in both domains. An exact analytical expression for the bit error probability (BEP) is necessary to analyze accurately the performance of Alamouti-coded OFDM systems over the spatio-temporally correlated UWA channel model. Hence, by using this UWA channel model, an expression has been derived for the BEP of Alamouti-coded OFDM systems assuming that the receiver knows perfectly the channel state information. The BEPs of two special cases are also studied, where the UWA channel is only correlated in either time or space. The performance of the Alamouti-coded OFDM system over UWA channels has been assessed for different maximum Doppler frequencies and antenna spacings. All theoretical results are validated by system simulations.

Index terms — Underwater acoustic channels, bit error probability, Alamouti scheme, orthogonal frequency division multiplexing, space time block coding.

I. INTRODUCTION

Multiple-input multiple-output orthogonal frequency division multiplexing (MIMO OFDM) systems, which are very advantageous for band-limited underwater acoustic (UWA) channels, have been thoroughly investigated in recent years [1], [2]. Space-time block coding (STBC) techniques such as the Alamouti scheme [3] coupled with OFDM provides more reliable communications with high data rate transmissions [4].

The application of the simple Alamouti scheme in UWA communication systems has been extensively studied in the literature [5]–[7]. For example, in [5], a detection algorithm has been proposed for UWA communication systems exploiting the Alamouti STBC scheme. In contrast, two different detection algorithms have been proposed in [6] and [7] for UWA communication systems by employing Alamouti space-frequency block coding (SFBC) techniques.

It is shown in [8] that the Alamouti scheme performs well if the channel remains constant over the duration of an Alamouti codeword. Owing to the fact that UWA channels cannot be assumed to be constant over the duration of two consecutive OFDM blocks [5], there is a need to study the degradation effect of the temporal correlation of UWA channels on the performance of Alamouti-coded OFDM systems for UWA communications. This effect has been investigated in [9]–[12] for mobile radio communications over Rayleigh fading channels. It has been shown in [10] by simulation and in [11] and [12] by theory that the performance of Alamouti STBC OFDM systems depends on both the temporal correlation and the spatial correlation of the 2-by-1 channel. For an accurate performance analysis of communication systems over spatio-temporally correlated UWA channels, the exact theoretical expression for the bit error probability (BEP) is required.

In this paper, we first extend the UWA channel model developed in [13] with respect to spatial selectivity. Then, we study the performance of Alamouti-coded OFDM systems over the proposed UWA channel model, which is correlated in time and space. The performance is assessed by taking into account that the UWA channel varies during two consecutive transmission time slots. Starting from the instantaneous output signal-to-interference-plus-noise ratio (SINR), we derive a general exact expression for the BEP. This expression is then used to study the performance for several specific cases, where the channel is correlated in time or space or even in both domains. The general expression is not limited to UWA channels. In fact, it can also be used for analyzing the performance of any time-varying multipath Rayleigh fading channel. It needs to mention that the detection scheme used in this paper is different from those of the aforementioned in [9]–[12]. The obtained results allow us to study the influence of the antenna spacing and maximum Doppler frequency on the system performance. It will be shown that the performance of Alamouti-coded OFDM systems depends greatly on the statistics of the UWA channel assessed at the antenna spacing and symbol duration.

The rest of this paper is structured as follows. Sections II and III represent the geometrical model and the therefrom derived UWA channel model, respectively. In Section IV, the Alamouti scheme and the symbol detection method are reviewed. The performance of Alamouti-coded OFDM systems over the proposed UWA channel model is studied in Section V. In Section VI, some numerical results are presented. Finally, the conclusions are drawn in Section VII.
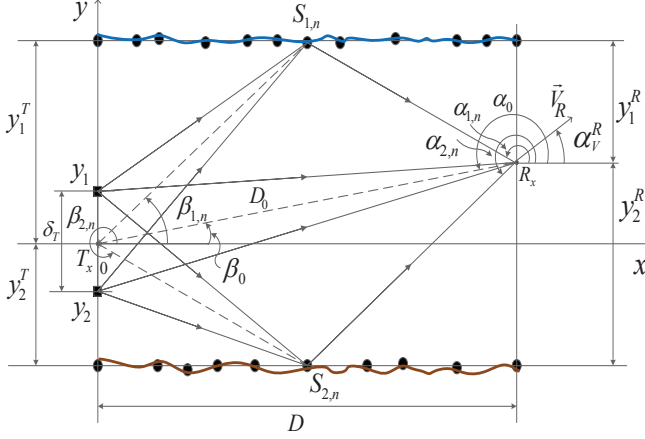
Fig. 1. A geometrical scattering model for a UWA channel with N_i^S randomly distributed scatterers $S_{i,n}(\bullet)$ $(n = 1, 2, \ldots, N_i^S)$ on the surface $(i = 1)$ and bottom $(i = 2)$ of the ocean.

II. THE GEOMETRICAL UWA MODEL

In this paper, we first extend the 1-by-1 UWA channel model presented in [13] to a 2-by-1 channel to make it readily available for systems with two transmit antennas and one receiver antenna. Fig. 1 presents the geometrical scattering model for UWA communication channels assuming that the scatterers $S_{i,n}$ $(n = 1, 2, \ldots, N_i^S$ and $i = 1, 2)$ are uniformly distributed on the surface $(i = 1)$ and bottom $(i = 2)$ of the ocean between the transmitter and the receiver. Moreover, single-bounce scattering is assumed, i.e., each transmitted acoustic signal arrives at the receiver after a single bounce on the surface or bottom of the ocean. The fixed transmitter T_x is positioned at y_1^T and y_2^T seen from the surface and bottom of the ocean, respectively. Moreover, the transmitter T_x is equipped with two omnidirectional acoustic antennas separated by the antenna distance δ_T. The single hydrophone receiver R_x is located at the distance y_1^R and y_2^R from the surface and bottom of the ocean, respectively. We assume that the receiver R_x is moving with constant velocity $\vec{v}_R$ in the direction determined by the angle-of-motion (AOM) α_v^R. According to Fig. 1, the distance along the x-axis between T_x and R_x is denoted by D. The symbol $\alpha_{i,n}(\beta_{i,n})$ denotes the angle-of-arrival (AOA) (angle-of-departure (AOD)) of the nth path associated with the ocean's surface $(i = 1)$ and the bottom $(i = 2)$. The symbol α_0 (β_0) stands for the AOA (AOD) of the line-of-sight (LOS) component. Finally, the parameter D_0 denotes the total distance which the LOS component travels from T_x to R_x.

III. UWA CHANNEL MODEL

In this section, we present first the complex space-time variant channel transfer function (STVCTF) of the UWA channel model, and then we study the correlation functions of the UWA channel model required for the performance analysis of MIMO-OFDM UWA communication systems.

A. The STVCTF of the UWA Channel Model

The function $H_{k1}(f', y_k, t_m)$ represents the STVCTF of the transmission link between the kth transmit antenna located at y_k $(k = 1, 2)$ and the single receive antenna at the time slot t_m $(m = 1, 2)$. We assume that the real and imaginary parts of $H_{k1}(f', y_k, t_m)$ are uncorrelated, each having the variance σ_0^2. The STVCTFs $H_{k1}(f', y_k, t_m)$ can be presented by their envelopes $R_p = |H_{k1}(f', y_k, t_m)|$ and phases $\Theta_p = \arg\{H_{k1}(f', y_k, t_m)\}$ for $p = 1, 2, 3,$ and 4 as follows

$$H_{11}(f', y_1, t_1) = R_1 e^{j\Theta_1}, \quad H_{11}(f', y_1, t_2) = R_2 e^{j\Theta_2}$$
$$H_{21}(f', y_2, t_1) = R_3 e^{j\Theta_3}, \quad H_{21}(f', y_2, t_2) = R_4 e^{j\Theta_4}. \quad (1)$$

According to the geometrical model illustrated in Fig. 1, the STVCTF $H_{k1}(f', y_k, t_m)$ can be split into three parts. The first part $H_{0,k}(f', y_k, t_m)$ is associated with the LOS component, whereas the second part $H_{1,k}(f', y_k, t_m)$ and the third part $H_{2,k}(f', y_k, t_m)$ are determined by the scattered components from the surface and bottom of the ocean, respectively. Thus, the STVCTF $H_{k1}(f', y_k, t_m)$ can be expressed by

$$H_{k1}(f', y_k, t_m) = \sum_{i=0}^{2} H_{i,k}(f', y_k, t_m) \quad (2)$$

where $k = 1, 2$ and $m = 1, 2$.

The LOS part $H_{0,k}(f', y_k, t_m)$ of the STVCTF is given by

$$H_{0,k}(f', y_k, t_m) = \sqrt{\frac{c_R}{1 + c_R}} \, c_0 \, e^{j[2\pi(f_0 t_m - f'\tau_0') + \theta_0]}$$
$$\cdot e^{-j[\frac{2\pi}{\lambda} D_{0,k}]} \quad (3)$$

in which c_R is the Rice factor, and the quantities c_0, τ_0', and θ_0 denote the gain, delay, and the phase shift of the LOS component, respectively. The parameter λ designates the wavelength, which is determined by $\lambda = c_s/f_c$, where c_s and f_c are the speed of sound and the central carrier frequency, respectively. The symbol $D_{0,k}$ stands for the total distance which the transmitted signal travels from the kth transmit acoustic antenna to the receiver hydrophone. This quantity is given by

$$D_{0,k} = D_0 + \frac{\delta_T(3 - 2k)}{2} \sin(\beta_0), \quad k = 1, 2. \quad (4)$$

The Doppler frequency f_0 in (3) is determined by

$$f_0 = f_{\max}^R \cos(\alpha_0 - \alpha_v^R) \quad (5)$$

where $f_{\max}^R$ is the maximum Doppler frequency associated with the receiver R_x.

The second part $H_{1,k}(f', y_k, t_m)$ and the third part $H_{2,k}(f', y_k, t_m)$ of the STVCTF $H_{k1}(f', y_k, t_m)$ in (2) are given by

$$H_{i,k}(f', y_k, t_m) = \frac{1}{\sqrt{1 + c_R}} \sum_{n=1}^{N_i^S} c_{i,n} \, e^{j[2\pi(f_{i,n}t_m - f'\tau_{i,n}') + \theta_{i,n}]}$$
$$\cdot e^{-j[\frac{2\pi}{\lambda} D_{i,n,k}]} \quad (6)$$

for $i = 1, 2$, where $c_{i,n}$, $f_{i,n}$, $\tau_{i,n}'$ and $\theta_{i,n}$, denote, respectively, the gains, Doppler shifts, delays, and the phase shifts

of the nth received component from the surface ($i = 1$) and bottom ($i = 2$) of the ocean. The parameter $D_{i,n,k}$ stands for the total distance which the transmitted signal travels from the kth transmit antenna to the receive antenna after the interaction with the nth scatterer on the surface ($i = 1$) and bottom ($i = 2$) of the ocean. This parameter can be expressed by

$$D_{i,n,k} = \frac{(-1)^{(i-1)} y_i^T}{\sin(\beta_{i,n})} + \frac{(-1)^{(i-1)} y_i^R}{\sin(\alpha_{i,n})} + \frac{\delta_T(3 - 2k)}{2} \sin(\beta_{i,n}) \tag{7}$$

for $i, k = 1, 2$ and $n = 1, 2, \ldots, N_i^S$.

B. Correlation Functions of the UWA Channel Model

In this section, we define the correlation functions of the UWA channel model, such as the space-time cross-correlation function (CCF), temporal autocorrelation function (ACF), and the space CCF. The space-time CCF $r_{HH}(\delta_T, \tau)$ of the subchannels $H_{11}(f', y_1, t_1)$ and $H_{21}(f', y_2, t_2)$ is defined by

$$r_{HH}(\delta_T, \tau) = E\{H_{11}^*(f', y_1, t_1) \cdot H_{21}(f', y_2, t_2)\} \tag{8}$$

where $()^*$ and $E\{\cdot\}$ represent the complex conjugate operation and the statistical expectation operator, respectively. The quantity $\tau = t_2 - t_1$ denotes the time separation variable and $\delta_T = y_2 - y_1$ denotes the antenna spacing. According to the generalized principle of deterministic channel modelling [14, pp. 418], a stochastic simulation model can be derived by using only a finite number of scatterers $S_{i,n}$ and placing them at fixed positions on the surface ($i = 1$) and the bottom ($i = 2$) of the ocean. Without proof, we mention that the resulting space-time CCF $\hat{r}_{HH}(\delta_T, \tau)$ of the simulation UWA channel model can be computed as

$$\hat{r}_{HH}(\delta_T, \tau) = \frac{c_R}{1 + c_R} c_0^2 \, e^{j2\pi[f_0\tau - \frac{\delta_T}{\lambda}\sin(\beta_0)]}$$

$$+ \frac{1}{1 + c_R} \sum_{i=1}^{2} \sum_{n=1}^{N_i^S} c_{i,n}^2 \, e^{j2\pi[f_{i,n}\tau - \frac{\delta_T}{\lambda}\sin(\beta_{i,n})]}. \tag{9}$$

For the parametrization of the channel simulator, i.e., obtaining the channel simulator parameters including $c_{i,n}, f_{i,n}, \beta_{i,n}$, and $\alpha_{i,n}$, we employ the parameter computation method, which is called the method of equally spaced scatterers (MESS) [13]. It should be noted that the temporal ACF $\hat{r}HH(\tau)$ and the space CCF $\hat{r}_{HH}(\delta_T)$ are obtained from the space-time CCF $\hat{r}_{HH}(\delta_T, \tau)$ by setting τ and δ_T to zero, respectively, i.e., $\hat{r}_{HH}(\tau) = \hat{r}_{HH}(0, \tau)$ and $\hat{r}_{HH}(\delta_T) = \hat{r}_{HH}(\delta_T, 0)$.

IV. Review of the Alamouti-Coded OFDM system

As mentioned in Section II, in this paper, an OFDM system equipped with two transmit antennas and one receive antenna is considered. A complex data symbol pair (S_1, S_2) is encoded first by means of the Alamouti scheme, and then it is transmitted over a UWA channel. The received symbols Y_1 and Y_2 at the time slots t_1 and t_2, respectively, can be expressed in matrix form as

$$\begin{bmatrix} Y_1 \\ Y_2^* \end{bmatrix} = \begin{bmatrix} H_{11}(f', y_1, t_1) & H_{21}(f', y_2, t_1) \\ H_{21}^*(f', y_2, t_2) & -H_{11}^*(f', y_1, t_2) \end{bmatrix} \begin{bmatrix} S_1 \\ S_2 \end{bmatrix} + \begin{bmatrix} N_1 \\ N_2^* \end{bmatrix}. \tag{10}$$

where N_m denotes a zero-mean additive underwater noise component at the time slot $t_m \, (m = 1, 2)$. Thus, we have equivalently

$$\mathbf{Y} = \mathbf{HS} + \mathbf{N} \tag{11}$$

in which $\mathbf{H}$ denotes the 2-by-2 channel matrix, and $\mathbf{N}$ is the noise vector. The symbol $\mathbf{S}$ and $\mathbf{Y}$ are the transmitted symbol vector and received symbol vector, respectively. Under the assumption that the receiver knows perfectly the channel state information and there is no synchronization error, the symbol vector $\mathbf{S}$ can be estimated as [15]

$$\hat{\mathbf{S}} = \mathbf{H^H Y} = \mathbf{H^H HS} + \mathbf{H^H N} \tag{12}$$

where $\mathbf{H^H}$ is the conjugate transpose of the channel matrix $\mathbf{H}$. Thus, the estimated symbols $\hat{S}_1$ and $\hat{S}_2$ at the output of the combiner can be expressed by (13a) and (13b) (see (13) at the bottom of the next page). As can be seen from (13a) and (13b), each estimated symbol experiences intersymbol-interference (ISI). But, due to the fact that the space CCFs $E\{H_{11}^*(f', y_1, t_1)H_{21}(f', y_2, t_1)\}$ and $E\{H_{11}^*(f', y_1, t_2)H_{21}(f', y_2, t_2)\}$ are equal, no diversity order is lost in the system [15].

V. Performance Analysis of Alamouti-Coded OFDM Systems

In this section, we first analyze the instantaneous output SINR, and then we study the BEP of the Alamouti-coded OFDM system over UWA channels.

A. The Instantaneous Output SINR

Due to the fact that the system model is symmetrical, the BEPs of S_1 and S_2 are equal. Thus, it is sufficient if we only focus on analyzing the BEP of S_1. From (13a), the instantaneous output SINR γ_Σ of S_1 can be expressed as (14) (see (14) at the bottom of the next page), in which $2\sigma_n^2$ represents the variance of the noise.

B. The Joint Probability Density Function of the Envelopes

An expression for the joint probability density function (PDF) of the envelopes R_1, R_2, R_3, and R_4 is required for the performance analysis. In [12], the joint PDF $p_{R_1 R_2 R_3 R_4}(r_1, r_2, r_3, r_4)$ of four envelopes has been derived. The obtained expression (see [12, Eq. (16)]) is represented at the bottom of the next page (see (15)), where the symbols A, B, C, D, and E are given by [12, Eq. (13)]

$$A = 2\rho_T\rho_x\rho_{x,T} + \sigma_0^2(\sigma_0^4 - \rho_T^2 - \rho_x^2 - \rho_{x,T}^2), \tag{16a}$$

$$B = 2\sigma_0^2\rho_x\rho_{x,T} - \rho_T(\sigma_0^4 - \rho_T^2 + \rho_x^2 + \rho_{x,T}^2), \tag{16b}$$

$$C = 2\sigma_0^2\rho_T\rho_{x,T} - \rho_x(\sigma_0^4 + \rho_T^2 - \rho_x^2 + \rho_{x,T}^2), \tag{16c}$$

$$D = 2\sigma_0^2\rho_T\rho_x - \rho_{x,T}(\sigma_0^4 + \rho_T^2 + \rho_x^2 - \rho_{x,T}^2), \tag{16d}$$

$$\begin{aligned} E &= (\sigma_0^4 - \rho_T^2)^2 + (\rho_x^2 - \rho_{x,T}^2)^2 \\ &\quad - 2(\sigma_0^4 + \rho_T^2)(\rho_x^2 + \rho_{x,T}^2) + 8\sigma_0^2\rho_T\rho_x\rho_{x,T} \end{aligned} \tag{16e}$$

respectively, where $\rho_T = r_{HH}(T_s)/2$, $\rho_x = r_{HH}(\delta_T)/2$, and $\rho_{x,T} = r_{HH}(\delta_T, T_s)/2$. The symbol T_s denotes the OFDM symbol duration.

C. Derivation of the PDF of the Instantaneous Output SINR

It is shown in [11] that the differences between the phase changes $\Theta_3 - \Theta_1$ and $\Theta_4 - \Theta_2$ can be neglected, i.e., $\Theta_3 - \Theta_1 - (\Theta_4 - \Theta_2) \approx 0$. This allows us to approximate the instantaneous output SINR γ_Σ as

$$\gamma_\Sigma \approx \frac{(R_1^2 + R_4^2)^2}{(R_1 R_3 - R_2 R_4)^2 + 2\sigma_n^2 \cdot (R_1^2 + R_4^2)}. \tag{17}$$

To obtain the PDF $p_{\gamma_\Sigma}(\gamma)$ of the instantaneous output SINR presented in (17), we define a system of equations as follows:

$$\begin{aligned} z_1 &= (r_1^2 + r_4^2)^2 \\ z_2 &= (r_1 r_3 - r_2 r_4)^2 + 2\sigma_n^2 \cdot (r_1^2 + r_4^2) \\ &= (z_3 - r_2 r_4)^2 + 2\sigma_n^2 \cdot \sqrt{z_1} \\ z_3 &= r_1 r_3, \qquad z_4 = r_1^2. \end{aligned} \tag{18}$$

This system of equations has the following real-valued solutions under the preconditions that $z_3 > \sqrt{z_2 - 2\sigma_n^2 \cdot \sqrt{z_1}}$, $z_4 < \sqrt{z_1}$, and $z_2 > 2\sigma_n^2 \cdot \sqrt{z_1}$:

$$\begin{aligned} r_1 &= \sqrt{z_4}, \qquad r_2 = \frac{z_3 - \sqrt{z_2 - 2\sigma_n^2 \cdot \sqrt{z_1}}}{\sqrt{\sqrt{z_1} - z_4}} \\ r_3 &= \frac{z_3}{\sqrt{z_4}}, \qquad r_4 = \sqrt{\sqrt{z_1} - z_4}. \end{aligned} \tag{19}$$

The joint PDF of the random variables Z_1, Z_2, Z_3, and Z_4 can be obtained by applying the concept of transformation of random variables [16, p. 244]. Thus,

$$\begin{aligned} &p_{Z_1 Z_2 Z_3 Z_4}(z_1, z_2, z_3, z_4) = |J(z_1, z_2, z_3, z_4)| \\ &\cdot p_{R_1 R_2 R_3 R_4}\left(\sqrt{z_4}, \frac{z_3 - \sqrt{z_2 - 2\sigma_n^2 \cdot \sqrt{z_1}}}{\sqrt{\sqrt{z_1} - z_4}}, \frac{z_3}{\sqrt{z_4}}, \sqrt{\sqrt{z_1} - z_4}\right) \end{aligned} \tag{20}$$

where $J(z_1, z_2, z_3, z_4)$ denotes the Jacobian determinant, which can be expressed as

$$J(z_1, z_2, z_3, z_4) = \frac{1}{16(z_1 z_4 - z_4^2\sqrt{z_1}) \cdot \sqrt{z_2 - 2\sigma_n^2 \cdot \sqrt{z_1}}}. \tag{21}$$

Now, integrating the joint PDF $p_{Z_1 Z_2 Z_3 Z_4}(z_1, z_2, z_3, z_4)$ over the variables z_3 and z_4 results in the joint PDF $p_{Z_1 Z_2}(z_1, z_2)$ of the random variables Z_1 and Z_2, which is presented in (22) at the bottom of the next page. By applying the rule presented in [16, Eq. (6–59)], the PDF of the random variable $\gamma_\Sigma = Z_1/Z_2$ can be expressed in terms of the joint PDF $p_{R_1 R_2 R_3 R_4}(r_1, r_2, r_3, r_4)$ as

$$\begin{aligned} p_{\gamma_\Sigma}(\gamma) = \frac{1}{16} \int\limits_{4\sigma_0^4\gamma/\bar{\gamma}^2}^{\infty} \int\limits_{\zeta}^{\infty} \int\limits_{0}^{\omega} \frac{z_2}{(\omega^2 z_4 - \omega z_4^2) \cdot \zeta} \\ \cdot p_{R_1 R_2 R_3 R_4}\left(\sqrt{z_4}, \frac{z_3 - \zeta}{\sqrt{\omega - z_4}}, \frac{z_3}{\sqrt{z_4}}, \sqrt{\omega - z_4}\right) dz_4 dz_3 dz_2 \end{aligned} \tag{23}$$

where ζ and ω are defined as $\zeta = \sqrt{z_2 - 2\sigma_0^2\omega/\bar{\gamma}}$ and $\omega = \sqrt{\gamma z_2}$, respectively. The variance $2\sigma_n^2$ of the noise in (22) has been replaced by $2\sigma_n^2 = 2\sigma_0^2/\bar{\gamma}$ in which the parameter $\bar{\gamma}$ stands for the average signal-to-noise ratio (SNR). As can be seen in (23), the precondition $z_2 > 2\sigma_n^2 \cdot \sqrt{z_1}$ results in $z_2 > 4\sigma_0^4\gamma/\bar{\gamma}^2$.

$$\begin{aligned} \hat{S}_1 &= [|H_{11}(f', y_1, t_1)|^2 + |H_{21}(f', y_2, t_2)|^2]S_1 + [H_{11}^*(f', y_1, t_1)H_{21}(f', y_2, t_1) - H_{11}^*(f', y_1, t_2)H_{21}(f', y_2, t_2)]S_2 \\ &\quad + H_{11}^*(f', y_1, t_1)N_1 + H_{21}(f', x_{T_2}, t_2)N_2^* \end{aligned} \tag{13a}$$

$$\begin{aligned} \hat{S}_2 &= [|H_{11}(f', y_1, t_2)|^2 + |H_{21}(f', y_2, t_1)|^2]S_2 + [H_{11}(f', y_1, t_1)H_{21}^*(f', y_2, t_1) - H_{11}(f', y_1, t_2)H_{21}^*(f', y_2, t_2)]S_1 \\ &\quad + H_{21}^*(f', y_2, t_1)N_1 - H_{11}(f', y_1, t_2)N_2^* \end{aligned} \tag{13b}$$

$$\gamma_\Sigma = \frac{(R_1^2 + R_4^2)^2}{(R_1 R_3)^2 + (R_2 R_4)^2 - 2R_1 R_2 R_3 R_4 \cos(\Theta_3 - \Theta_1 + \Theta_2 - \Theta_4) + 2\sigma_n^2 \cdot (R_1^2 + R_4^2)} \tag{14}$$

$$\begin{aligned} p_{R_1 R_2 R_3 R_4}(r_1, r_2, r_3, r_4) = \frac{r_1 r_2 r_3 r_4}{(2\pi)^2 E} e^{[-\frac{A}{2E}(r_1^2 + r_2^2 + r_3^2 + r_4^2)]} \int\limits_{0}^{2\pi} \int\limits_{0}^{2\pi} e^{-\frac{1}{E}[Br_3 r_4 \cos(\varphi_2) + Cr_2 r_4 \cos(\varphi_1 + \varphi_2) + Dr_2 r_3 \cos(\varphi_1)]} \\ \times I_0\left(\frac{r_1}{E}\sqrt{B^2 r_2^2 + C^2 r_3^2 + D^2 r_4^2 + 2[BCr_2 r_3 \cos(\varphi_1) + BDr_2 r_4 \cos(\varphi_1 + \varphi_2) + CDr_3 r_4 \cos(\varphi_2)]}\right) d\varphi_1 d\varphi_2 \end{aligned} \tag{15}$$

D. Derivation of the BEP

The instantaneous output BEP of the system can be obtained by using [17, Eq. (7.2)]

$$P_b = \int_0^\infty p_{\gamma_\Sigma}(\gamma) P_{b|\gamma_\Sigma}(\gamma) d\gamma \qquad (24)$$

where $P_{b|\gamma_\Sigma}(\gamma)$ denotes the conditional BEP of a digital modulation scheme for a specific value of γ. For example, for the binary phase shift keying (BPSK) modulation scheme, $P_{b|\gamma_\Sigma}(\gamma)$ is given by $P_{b|\gamma_\Sigma}(\gamma) = \mathrm{erfc}(\sqrt{\gamma})/2$, where $\mathrm{erfc}(x)$ denotes the complementary error function. Thus, the BEP P_b of the Alamouti-coded OFDM system can be computed by means of

$$P_b = \frac{1}{2} \int_0^\infty p_{\gamma_\Sigma}(\gamma) \mathrm{erfc}(\sqrt{\gamma}) d\gamma . \qquad (25)$$

Now, by inserting (15) in (23), and then substituting $p_{\gamma_\Sigma}(\gamma)$ in (25), we obtain the desired exact solution of the BEP of BPSK Alamouti-coded OFDM systems as shown in (26) (see the bottom of this page). The function $I_0(\cdot)$ in (26) is the zeroth-order modified Bessel function of the first kind. In the following, we will discuss two special cases where the UWA channel is correlated either in time or space. If we set $\rho_x = \rho_{x,T} = 0$ and $\rho_T \neq 0$, then the BEP in (26) reduces to

$$P_b = \frac{1}{32(\sigma_0^4 - \rho_T^2)} \int_0^\infty \int_{4\sigma_0^4 \gamma/\bar{\gamma}^2}^\infty \int_\zeta^\infty \int_0^\omega \frac{z_2 z_3 (z_3 - \zeta)}{(\omega^2 z_4 - \omega z_4^2) \cdot \zeta}$$
$$\cdot I_0 \left(\frac{\sqrt{z_4}(z_3 - \zeta)\rho_T}{\sqrt{\omega - z_4}(\sigma_0^4 - \rho_T^2)} \right) I_0 \left(\frac{z_3 \sqrt{\omega - z_4}\rho_T}{\sqrt{z_4}(\sigma_0^4 - \rho_T^2)} \right)$$
$$\cdot e^{-\frac{\sigma_0^2}{2(\sigma_0^4 - \rho_T^2)} \left[\frac{(z_3 - \zeta)^2}{\omega - z_4} + \omega + \frac{z_3^2}{z_4} \right]} \mathrm{erfc}(\sqrt{\gamma}) dz_4 dz_3 dz_2 d\gamma \qquad (27)$$

which presents the performance of the Alamouti-coded OFDM system over a UWA channel that is only correlated in time. Analogously, if we consider the Alamouti-coded OFDM system over the UWA channel that is only correlated in space, i.e., $\rho_T = \rho_{x,T} = 0$ and $\rho_x \neq 0$, then the BEP in (26) reduces to

$$P_b = \frac{1}{32(\sigma_0^4 - \rho_x^2)} \int_0^\infty \int_{4\sigma_0^4 \gamma/\bar{\gamma}^2}^\infty \int_\zeta^\infty \int_0^\omega \frac{z_2 z_3 (z_3 - \zeta)}{(\omega^2 z_4 - \omega z_4^2) \cdot \zeta}$$
$$\cdot I_0 \left(\frac{z_3 \rho_x}{\sigma_0^4 - \rho_x^2} \right) I_0 \left(\frac{(z_3 - \zeta)\rho_x}{\sigma_0^4 - \rho_x^2} \right)$$
$$\cdot e^{-\frac{\sigma_0^2}{2(\sigma_0^4 - \rho_x^2)} \left[\frac{(z_3 - \zeta)^2}{\omega - z_4} + \omega + \frac{z_3^2}{z_4} \right]} \mathrm{erfc}(\sqrt{\gamma}) dz_4 dz_3 dz_2 d\gamma . \qquad (28)$$

VI. Numerical Results

In this section, we illustrate the theoretical BEP results presented in (26), (27), and (28) for different maximum Doppler frequencies $f_{\max}^R$ and different normalized transmit hydrophone spacings δ_T/λ. The correctness of the theoretical results has been confirmed by system simulations. In the simulation setup, an OFDM system with $K = 64$ subcarriers and channel bandwidth $B = 4000\,\mathrm{Hz}$ is considered. The symbol duration T_s equals $16\,\mathrm{ms}$, and the central carrier frequency f_c has been set to $10\,\mathrm{kHz}$. The speed of sound c_s is assumed to be 1500 m/s which results in a wavelength λ of 15 cm. The remaining parameters have been set as follows: $y_1^T = y_2^T = y_1^R = y_2^R = 50\,\mathrm{m}$, $D = 1\,\mathrm{km}$ and $\alpha_v^R = 0$. As mentioned in Section III-B, for the parametrization of the UWA channel simulator the MESS has been used.

The BEP performance of the Alamouti-coded OFDM system over the spatio-temporally correlated UWA channel is shown in Fig. 2 for different maximum Doppler frequencies $f_{\max}^R$ and different hydrophone spacings δ_T. It can be

---

$$p_{Z_1 Z_2}(z_1, z_2) = \int_{\sqrt{z_2 - 2\sigma_n^2 \cdot \sqrt{z_1}}}^\infty \int_0^{\sqrt{z_1}} \frac{1}{16(z_1 z_4 - z_4^2 \sqrt{z_1}) \cdot \sqrt{z_2 - 2\sigma_n^2 \cdot \sqrt{z_1}}}$$
$$\cdot p_{R_1 R_2 R_3 R_4} \left(\sqrt{z_4}, \frac{z_3 - \sqrt{z_2 - 2\sigma_n^2 \cdot \sqrt{z_1}}}{\sqrt{\sqrt{z_1} - z_4}}, \frac{z_3}{\sqrt{z_4}}, \sqrt{\sqrt{z_1} - z_4} \right) dz_4 dz_3 \qquad (22)$$

$$P_b = \frac{1}{128\pi^2 E} \int_0^\infty \int_{4\sigma_0^4 \gamma/\bar{\gamma}^2}^\infty \int_\zeta^\infty \int_0^\omega \frac{z_2 z_3 (z_3 - \zeta)}{(\omega^2 z_4 - \omega z_4^2) \cdot \zeta} \cdot e^{-\frac{A}{2E} \left[\frac{(z_3 - \zeta)^2}{\omega - z_4} + \omega + \frac{z_3^2}{z_4} \right]} \mathrm{erfc}(\sqrt{\gamma}) \int_0^{2\pi} \int_0^{2\pi}$$
$$I_0 \left(\frac{\sqrt{z_4}}{E} \left(B^2 \frac{(z_3 - \zeta)^2}{\omega - z_4} + C^2 \frac{z_3^2}{z_4} + D^2 (\omega - z_4) \right.\right.$$
$$\left.\left. + 2[BC \frac{(z_3^2 - \zeta z_3)}{\sqrt{z_4 \omega - z_4^2}} \cos\varphi_1 + BD(z_3 - \zeta)\cos(\varphi_1 + \varphi_2) + CD \frac{z_3 \sqrt{\omega - z_4}}{\sqrt{z_4}} \cos\varphi_2] \right)^{(1/2)} \right)$$
$$e^{-\frac{1}{E}[B \frac{z_3 \sqrt{\omega - z_4}}{\sqrt{z_4}} \cos\varphi_2 + C(z_3 - \zeta)\cos(\varphi_1 + \varphi_2) + D \frac{(z_3^2 - \zeta z_3)}{\sqrt{z_4 \omega - z_4^2}} \cos\varphi_1]} d\varphi_1 d\varphi_2 dz_4 dz_3 dz_2 d\gamma \qquad (26)$$
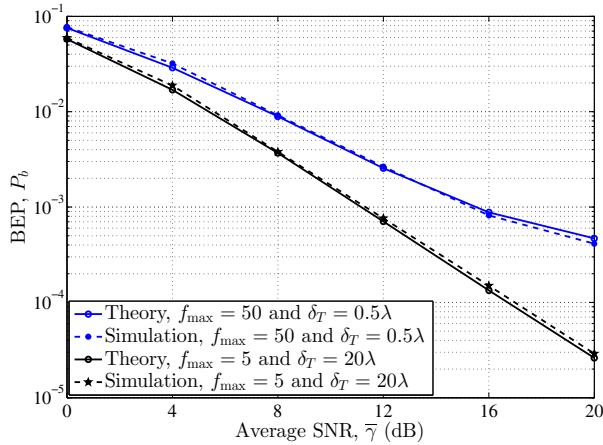
Fig. 2. The BEP performance of an Alamouti-coded OFDM system over an UWA channel correlated in space and time for different values of the maximum Doppler frequencies $f_{\max}^R = 5\,\text{Hz}$ and $f_{\max}^R = 50\,\text{Hz}$ and hydrophone spacing $\delta_T = 0.5\lambda$ and $\delta_T = 20\lambda$.

Fig. 4. The BEP performance of an Alamouti-coded OFDM system over UWA channels, which are only correlated in space for different values of the hydrophone spacing $\delta_T = 0.5\lambda$ and $\delta_T = 20\lambda$.

VII. CONCLUSION

In this paper, the performance of Alamouti-coded OFDM systems over a proposed UWA channel correlated in time and/or space has been analyzed. The channel envelope can change during two consecutive transmission time slots which accounts for realistic UWA propagation scenarios. An exact analytical expression for the BEP of the system has been derived for a spatio-temporally correlated UWA channel. The derived expression for the BEP has been reduced to the special cases that the UWA channel is either correlated in time or correlated in space. The simulation results show that the performance of Alamouti-coded OFDM systems over the UWA channel depends strongly on the value of the STVCTF evaluated at the symbol duration and the antenna separation.
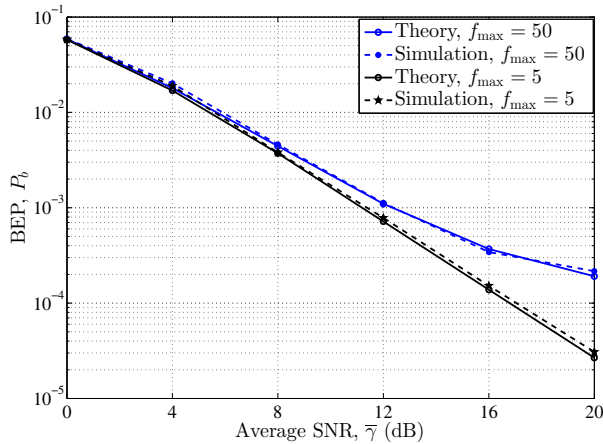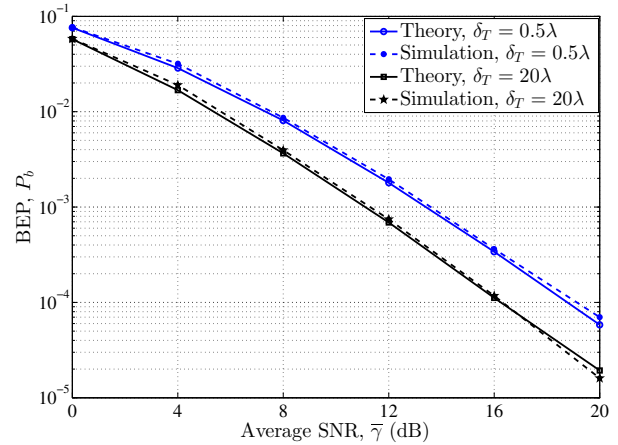

Fig. 3. The BEP performance of an Alamouti-coded OFDM system over UWA channels, which are only correlated in time for different values of the maximum Doppler frequencies $f_{\max}^R = 5\,\text{Hz}$ and $f_{\max}^R = 50\,\text{Hz}$.

concluded that both the maximum Doppler frequencies and hydrophone spacing influence the system performance. With reference to Fig. 2, the BEP described in (26) fits closely to the one obtained by simulations.

Fig. 3 illustrates the BEP performance of an Alamouti-coded OFDM system for the special case where the UWA channel is only correlated in time for $f_{\max}^R = 5\,\text{Hz}$ and $f_{\max}^R = 50\,\text{Hz}$ (see (27)). As can be seen in this figure, the BEP performance experiences a degradation if the maximum Doppler frequency $f_{\max}^R$ increases.

For the special case that the UWA channel is only correlated in space, the BEP performance of Alamouti-coded OFDM systems is depicted in Fig. 4 for different hydrophone spacings $\delta_T = 0.5\lambda$ and $\delta_T = 20\lambda$ (see (28)). From this figure, we can conclude that the performance improves if the hydrophone spacing δ_T increases. As can be observed in Figs. 3 and 4, the theoretical results have been validated by simulation results.

REFERENCES

[1] M. Stojanovic, "MIMO OFDM over underwater acoustic channels," in *Proc. IEEE Conf. on Signals, Syst. and Computers (ASILOMAR), 2010 Conf. Record of the Forty-Third Asilomar*, Nov. 2009, pp. 605–609.

[2] B. Li et al., "MIMO-OFDM for high-rate underwater acoustic communications," *IEEE J. Ocean. Eng.*, vol. 34, no. 4, pp. 634–644, Oct. 2009.

[3] S. M. Alamouti, "A simple transmit diversity technique for wireless communications," *IEEE J. Sel. Areas Commun.*, vol. 16, no. 8, pp. 1451–1458, Oct. 1998.

[4] T. M. Duman and A. Ghrayeb, *Coding for MIMO Communication Systems*, Chichester: John Wiley & Sons, 2007.

[5] B. Li and M. Stojanovic, "A simple design for joint channel estimation and data detection in an Alamouti OFDM system," in *OCEANS 2010*, Sept. 2010, pp. 1–5.

[6] E. V. Zorita and M. Stojanovic, "Space-frequency block coding for underwater acoustic communications," *IEEE J. Ocean. Eng.*, vol. 40, no. 2, pp. 303–314, Apr. 2015.

[7] H. Eghbali, M. Stojanovic, and S. Muhaidat, "Differential decoding for SFBC OFDM systems in underwater MIMO channels," in *Proc. IEEE International Conference on Acoustics, Speech and Signal Processing (ICASSP)*, May 2014, pp. 8102–8105.

[8] V. Tarokh, H. Jafarkhani, and A. R. Calderbank, "Space-time block coding for wireless communications: performance results," *IEEE J. Sel. Areas Commun.*, vol. 17, no. 3, pp. 451–460, Mar. 1999.

[9] E. Ko and D. Hong, "A robust transmit diversity for OFDM systems in spatially correlated Rayleigh fading channels," in *Proc. 59th IEEE Semiannual Veh. Technol. Conf., VTC 2004-Spring*, Milan, Italy, May 2004, vol. 4, pp. 1840–1843.

[10] Y. Ma and M. Pätzold, "Performance comparison of space-time coded MIMO-OFDM systems using different wideband MIMO channel models," in *Proc. 4th IEEE International Symposium on Wireless Communication Systems, ISWCS 2007*, Trondheim, Norway, Oct. 2007, pp. 762–766.

[11] Y. Ma and M. Pätzold, "Performance analysis of STBC-OFDM systems in temporally and spatially correlated fading channels," in *Proc. Wireless Communication and Network Conference, WCNC 2010*, Sydney, Australia, Apr. 2010.

[12] Y. Ma and M. Pätzold, "Performance analysis of Alamouti coded OFDM systems over Rayleigh fading channels correlated in space and time," in *Proc. IEEE 71st Vehicular Technology Conference, VTC2010-Spring*, Taipei, Taiwan, May 2010.

[13] M. Naderi, M. Pätzold, and A. G. Zajić, "A geometry-based channel model for shallow underwater acoustic channels under rough surface and bottom scattering conditions," in *Proc. 5th Int. Conf. on Commun. and Electron., ICCE 2014*, Da Nang, Vietnam, July/Aug. 2014, pp. 112–117.

[14] M. Pätzold, *Mobile Radio Channels*, Chichester: John Wiley & Sons, 2nd edition, 2011.

[15] G. Abreu and R. Kohno, "Non-differential space-time transmission diversity in fast fading," in *Proc. 13th IEEE Int. Symp. on Personal, Indoor and Mobile Radio Communications, PIMRC 2002*, Lisbon, Portugal, Sept. 2002, vol. 1, pp. 74–78.

[16] A. Papoulis, *Probability, Random Variables, and Stochastic Processes*, New York: McGraw-Hill, 4th edition, 2002.

[17] A. Goldsmith, *Wireless Communications*, Cambridge University Press, 2005.